Studies of EC pre-ionization in DIII-D to support development of ITER plasma initiation

J. Sinha[1,2*], P.C. de Vries[1], M.L. Walker[3], D.J. Battaglia[4], F. Turco[5], A. Hyatt[3], H.T. Kim[6], J. Stober[7], R. Yoneda[8], Y. Gribov[1], S.R. Haskey[4], I. Bykov[3], E. Hollmann[9], J.L. Herfindal[10], F. Glass[3], J. Chen[8], A. McLean[11] and the DIII-D team

1) ITER Organization, Route de Vinon-sur-Verdon, CS 90 046, 13067 St. Paul Lez Durance Cedex, France
2) Tokamak Energy Ltd., 173 Brook Drive, Milton Park, Oxfordshire, OX14 4SD, United Kingdom
3) General Atomics, San Diego, CA, USA
4) Princeton Plasma Physics Laboratory, Princeton, NJ, USA
5) Columbia University, New York, NY, USA
6) EUROfusion Programme Management Unit, Culham Science Centre, Abingdon, OX14 3DB, United Kingdom
7) Max-Planck-Institut für Plasmaphysik, Garching, Germany
8) University of California Los Angeles, Los Angeles, California 90095, USA
9) University of California San Diego, La Jolla, CA, 92093-0417, USA
10) Oak Ridge National Laboratory
11) Lawrence Livermore National Laboratory

Abstract

New experiments have been conducted at DIII-D to improve the physics understanding of plasma initiation assisted by Electron Cyclotron (EC) wave injection, allowing better extrapolation to ITER. This has been achieved by applying an EC pulse prior to start of the inductive plasma initiation (i.e. the generation of a loop voltage). A pre-plasma was formed during the EC pulse that was characterized in terms of the maximum density and temperature. Parametric scans were performed to study the influence of the EC injected power, EC injection angle, and pre-fill gas pressure on the pre-plasma creation process. These experiments showed that pre-ionized plasma of good quality can have a significant effect on the subsequent V_{loop} induced plasma initiation process, i.e. a high density pre-plasma, increases the plasma current

* Current affiliation

rise and speed at which ionization is achieved when the V_{loop} is applied. A good quality pre-plasma is one that achieved a significant degree of ionization, mainly obtained by providing sufficient ECH power in DIII-D of the order of 1 MW. It was found that a minimum EC power of 0.5 MW was required in DIII-D to create ionization, and this would scale to a minimum power of roughly 6.5 MW for ITER.

1. Introduction

Tokamak plasma initiation is generally achieved by inducing a toroidal electric field that ionizes a neutral gas and drives a toroidal current that, by ohmic heating, enhances the plasma temperature. The limited value of the toroidal electric field due to the thick vacuum vessel and superconducting coils ($E_{\Phi} \sim 0.3\ \mathrm{V/m}$) may complicate plasma initiation at ITER [1, 2]. Powerful electron cyclotron (EC) wave injection can assist plasma initiation (i.e. EC assist) by providing additional heating during the burn-through phase, but it is also able to pre-ionize the prefill gas [3-6]. The benefits of EC assist to tokamak plasma initiation are well known and have been applied successfully by many devices [3, 6, 7, 8, 9]. However, it is not easy to separate the beneficial impacts from the EC pre-ionization and the auxiliary heating provided during the burn-through process. New experiments have been carried out at DIII-D [10] to further improve the physics understanding of the effect of EC pre-ionization to allow better extrapolation to ITER.

Modelling of the ITER First Plasma (FP) burn-through process suggests that the impact of second harmonic EC is limited, due to the low fraction of EC power that is absorbed by the plasmas [2, 11]. The situation improves if one considers multi-pass absorption which will occur when the ITER blanket and first wall are installed after FP. Absorption also improves if first harmonic EC waves are used [2, 11]. It is however unclear which the detailed EC requirements are to create an EC pre-plasma, and how this pre-plasma is able to beneficially affect the overall plasma initiation process.

While the influence of EC heating on the burn-through process is well understood and can be modelled for ITER [12, 13], it is not clear how the experimental results for the pre-ionization process obtained at various devices extrapolate to ITER. To determine the requirements for ITER EC pre-ionization, a better understanding of the pre-ionization mechanism, and its effect on the subsequent inductive plasma initiation process is required [2]. Previous studies into EC pre-plasmas have shown that their formation is improved in the presence of a small vertical magnetic field component [3, 5, 6]. It was shown that EC pre-

plasmas can be formed that have significant electron densities, n_e, and temperatures, T_e (i.e. n_e >10^{18} m^{-3} and T_e>100 eV, respectively) and may even carry a toroidal current [4].

The process of the formation of EC pre-plasmas in tokamaks can be divided into four phases, namely: (1) the non-linear EC ionization phase, in which non-linear interaction between the electrons with the EC wave electric field is sufficiently large such that the energy transfer exceeds the energy needed to ionize the neutral particles in the pre-fill gas, (2) the electron multiplication phase, in which the plasma created near the overlap between the EC beam and the EC resonance expands toroidally along the magnetic field lines, thereby creating plasma in a narrow toroidal tube, (3) pre-plasma heating phase in which EC waves are absorbed by the plasma in the toroidal tubes, increasing its temperature, while plasma-neutral interaction further increases its degree of ionization, and finally (4) the expansion phase, when the plasma in the toroidal tubes expands into the entire volume, encompassing a large part of the tokamak vessel.

This entire process develops independently of whether a toroidal electric field is applied or not. A good physics model for the non-linear ionization phase is available [14]. This model predicts the minimum EC wave electric field strength needed to ionize the neutral gas, which can be converted to a minimum EC power density (i.e. the EC power P_{ECH}, per EC beam width, w_{EC}). This process is linked to the wave electric field, and not the total injected power. Adding EC from multiple launchers will increase the injected power but not necessarily the local wave-electric field, because the EC waves from different launchers are not synchronized. Hence, the exact specifics of the EC system used for a particular device are important for this phase. Based on the equations provided in ref. [14] the minimum second harmonic (X2) DIII-D EC power of 100 kW will be able to increase the electron energy into the range where the ionization cross-section is maximum (i.e., 60 eV). Note that this model does not explain which parameters will determine the development of the subsequent phases of the pre-ionization process; it would only generate ionization where the EC beam overlaps with the EC resonance.

As explained in ref. [3], the high pressure at this location will cause it to expand with the charged particles preferentially travelling along the toroidal field lines. This toroidal expansion happens on timescales related to the ion sound speed ($c_s = \sqrt{kT_e/m_i}$, where k is the Boltzmann constant, and m_i is the ion mass) as the high-pressure shock propagates toroidally. For DIII-D, this is expected to occur on a sub-millisecond timescale ($\sim \pi R_0/c_s$). Further ionization takes place in the toroidal tube via electron-neutral collisions. Once plasma is created, the EC wave-plasma absorption will further heat the plasma in the tube. The

temperature increase is, however, limited by various energy losses, amongst them the energy lost by neutral ionization. At one point, however, the majority of the neutrals may be ionized resulting in a fast increase of the plasma temperature. The high temperature plasma will diffuse away from the toroidal tube into the remainder of the vessel, initiating the final phase of the pre-plasma formation process. It was observed previously that this expansion process is not symmetric on both sides of the X2 resonance [4], suggesting it is heavily affected by a convection process. This whole process has much in common with that occurring in the formation of Electron Cyclotron Wall Conditioning (ECWC) plasmas generated for the purpose of cleaning the tokamak first wall [15].

The main questions that need to be answered are the following: 1) which of the previous phases of the EC pre-plasma development determine the effectiveness of ECH pre-ionization on plasma initiation? 2) What parameters, for example EC characteristics, prefill pressure or magnetic field configuration, affect these processes? 3) What parameters are best used to characterize the ECH pre-plasma? 4) How to quantify the effect of the EC pre-plasma on the V_{loop} induced plasma initiation process? And finally, 5) how can these results be extrapolated to ITER?

The new experiments performed in the DIII-D tokamak aim to understand the physics of all the four phases of the pre-ionization process as well as the impact of the pre-ionized plasma on the subsequent loop voltage (V_{loop}) induced plasma initiation process. These experiments build on the previous EC pre-plasma studies carried out at DIII-D [4-6] but focus on understanding the timescales involved in development of each of the phases, and importantly, how they influence the subsequent inductive plasma initiation process. These experiments were carried out on two different days separated by a long time period.

The experimental strategy used here differentiates from the previous studies into EC assisted plasma initiation by clearly separating the EC pre-ionization effects from EC heating during the burn-through phase. This is achieved by applying an EC pulse prior to the loop voltage application, with the end of the pulse corresponding to the onset of the loop voltage. With this experiment, the pure EC pre-ionization process can be studied, without it being influenced by the application of V_{loop}. Thereafter, the influence of this pre-plasma on the inductive plasma initiation can be studied.

Importantly, in this paper we consider two distinct aspects of burn-through. One of them is the burn-through phase of the impurities, which is the point during the V_{loop} induced plasma initiation at which the heating exceeds the losses due to ionization, impurity line-

radiation and bremsstrahlung [2]. The other aspect is the local main species burn-through, which is the point at which the local D_α emission peaks, suggesting that locally more than 50% of all neutrals have been ionized (i.e., $f_i = 0.5$) [2]. This is a local indicator and outside this local main species burn-through area a significant fraction of neutrals may remain.

In this paper, we will first introduce the experimental setup in Section 2, especially detailing the DIII-D ECH set-up used for these experiments and a number of other specifics relevant to the plasma initiation process. Moreover, the diagnostics utilized in the experiments are described. Diagnosing the plasmas at such an early stage in the discharge is not an easy task. It is therefore important to understand which diagnostics can be used and how exactly their results can be interpreted. Section 3 describes the experimental results obtained on the EC pre-plasma. Section 4 presents the results on the impact of the pre-ionized plasma on V_{loop} induced plasma initiation. Section 5 discusses the feasibility and implications of using EC-assisted start-up in ITER and, lastly, Section 6 presents the conclusions obtained from these experiments.

2. Experimental setup

As explained above, a clear separation between the formation of the EC pre-plasma and the inductive plasma initiation process was achieved at DIII-D using the pulse schedule shown in Figure 1. In DIII-D, the time t = 0 s corresponds to the expected creation of the plasma and all synchronous events (i.e., timing, system enables, etc.) needed for executing a pulse are defined with respect to this time. The neutral gas is injected into the vessel 300 ms prior to t = 0 s. The neutral gas pressure is measured using the ASDEX fast neutral pressure gauge [16] located at the midplane. Here, the prefill pressure corresponds to the measured value at the time the EC pulse was switched on. A 30 ms pulse of EC was injected prior to the application of the V_{loop}, during which the pre-plasma is formed. The vertical magnetic field configuration at that time was optimized for the use of EC assist, with a B_z = -2 mT, for a toroidal magnetic field of B_Φ = 1.8 T at the centre of the machine (i.e., at R_0 = 1.7 m) [4]. Thus, B_z was 0.1% of the central toroidal magnetic field. A V_{loop}, is applied at t = -9 ms and it reaches the maximum value of 4 V, at $t \sim 5$ ms as measured at the inboard midplane. This is equivalent to a toroidal electric field of E_Φ = 0.4 V/m, which is lower than in standard DIII-D operation. In these experiments V_{loop} has been feedback controlled. Without the ECH pre-plasma, the burn-through phase of the neutral gas (i.e., deuterium) typically takes place at $t \sim$ 15 to 25 ms, when applying V_{loop} = 4 V, as done in these experiments.

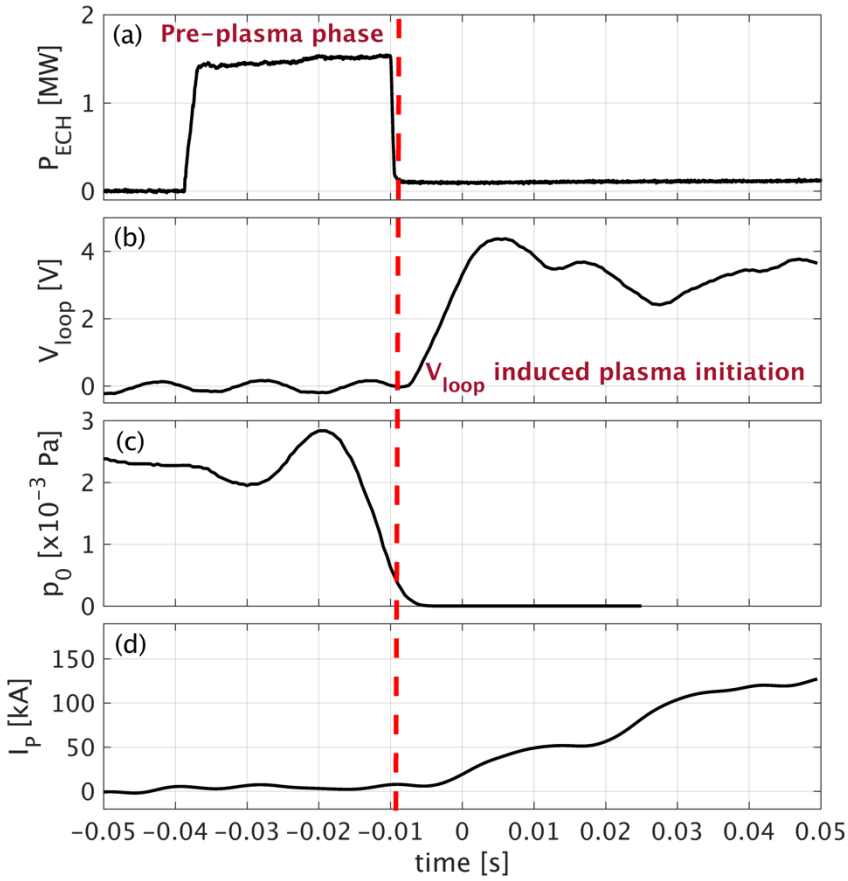

Figure 1: Typical set-up of a DIII-D pulse as used in the experiments described in this paper. Evolution of (a) injected ECH power (P_{ECH}), (b) applied V_{loop}, (c) measured prefill pressure, p_0, using the ASDEX neutral pressure gauge and (d) plasma current (I_{P}) during the EC pre-ionization phase and the V_{loop} induced plasma initiation phase. The red dashed line denotes the time when the EC pulse is switched off, separating the two parts of the experiment.

ECH beams are microwaves, with a frequency equal to the electron cyclotron frequency $\omega_{\mathrm{ce}} = eB/m_{\mathrm{e}}$, where B is therefore the local magnetic field where the waves are (first harmonic) resonant. These EC waves are resonant at a very specific radial location since the tokamak magnetic field strength varies as $1/R$. In these experiments, the dual EC launchers installed on DIII-D were used to inject second harmonic X-mode (X2) EC waves from the tokamak Low Field Side (LFS). The EC wave can be scanned toroidally up to ±20° and poloidally over 40° angular range in the tokamak upper half plane [17]. The EC beam width is ~10 cm at the plasma center [17]. Each launcher is connected to one gyrotron. In these experiments up to four 110 GHz gyrotrons, each having a nominal power of 500 kW, have been used to achieve EC pre-ionization. It should be noted that each single gyrotron has higher

power than the threshold proposed in [14]. In addition, more than one gyrotron is required to inject EC waves with P_{ECH} > 500 kW, which means that the power is injected at multiple toroidal locations.

Figure 2 shows an overview of the EC launchers and some of the essential diagnostics required for the characterization of the EC pre-ionization phase, illustrating their views or positions in the DIII-D tokamak. Figure 2a shows the top view, indicating the toroidal location of the ECH launchers with the EC beams injected at a toroidal angle of 0$^{\mathbf{o}}$ (solid blue lines) as well as the radial location where the EC beams will intersect at the X2 resonance layer. For 110 GHz EC with the B_{Φ} = 1.8 T, the resonance is located at R = 1.52 m.

The X2 mode EC single pass absorption in a plasma, scales with the product of n_{e} and T_{e} as long as n_{e} is far below cut-off [2]. Therefore, the higher the pre-ionized plasma density and temperature the higher the EC absorption. However, in this paper only the injected power has been used to characterize the EC pre-ionization process, since the fraction that is absorbed is small and not well known. The visible fast framing camera [18] is one of the important diagnostics able to provide information about the plasma time evolution of the different steps during the EC pre-ionization process (further details discussed in Section 3). The Field-of-View (FoV) of the fast-framing camera located in the 90$^{\mathbf{o}}$ platform in DIII-D is also shown in Figure 2a and it measures the line integrated emission along several Lines-of-Sight (LoS). It should be noted that the fast-framing camera does not look at the exact toroidal location where the EC wave intersects the X2 resonance layer. As a result, it can only provide useful measurements when the pre-ionized plasma has extended toroidally (i.e., once phase 2 of the EC pre-ionization process is completed).

Most of the diagnostics in tokamaks are optimized to measure high n_{e} and T_{e} so that the low values of these parameters associated with the EC pre-ionization process make it difficult to diagnose the plasma accurately. A limited set of diagnostics are able to provide measurements during the EC pre-ionization and V_{loop} induced plasma initiation phase. A poloidal view of the DIII-D tokamak illustrating the injected EC beam, the X2 resonance layer location and the LoS of different diagnostics is shown in Figure 2b. The LoS of the three vertical chords of the CO_2 interferometer, namely V1, V2 and V3 are located at R = 1.48 m, R = 1.94 m and R = 2.1 m respectively [19]. The interferometer measures the line integrated plasma density and for these experiments, the chord V1, which is located close to the X2 resonance layer location, has been used to measure the line-integrated pre-ionized plasma density ($n_{\mathrm{e,V1}}$) during the EC pre-ionization phase. However, it is difficult to determine the

path length of the V1 chord that passes through the pre-ionized plasma during the pre-ionization phase. Therefore, in order to determine the average pre-ionized plasma density along the V1 chord, the line-integrated density measurements are divided by the total path length of the laser beam passing through the vacuum vessel (~4.68 m). The interferometer can measure line-integrated density values above 5×10^{17} m^{-2}. Figure 2b also shows the radial interferometer polarimeter diagnostic that can also measure the line integrated density and is comprised three radial chords located at Z = -13.5 cm, Z = 0 cm and Z = 13.5 cm respectively [20].

The DIII-D Electron Cyclotron Emission (ECE) radiometer is a multichannel heterodyne system that can estimate the local T_e from measurements of optically thick, second harmonic (X-mode) electron cyclotron emission [21]. The ECE diagnostic has 40 channels which view along a horizontal chord at the tokamak mid-plane at a toroidal angle of 81° (Figure 2a). Some of the radial locations of this measurement, numbered from 5 to 40 are marked in Figure 2b. The optical thickness of the plasma during the EC pre-ionization phase is usually low, therefore it becomes difficult to accurately calibrate the ECE signals and estimate the absolute values of the local T_e. However, the ECE measurements can still be useful to examine the trends of the T_e during the EC pre-ionization phase. It should be noted that the measurements of T_e shown in the figures in this paper are measured using the ECE channels close to the resonance layer location.

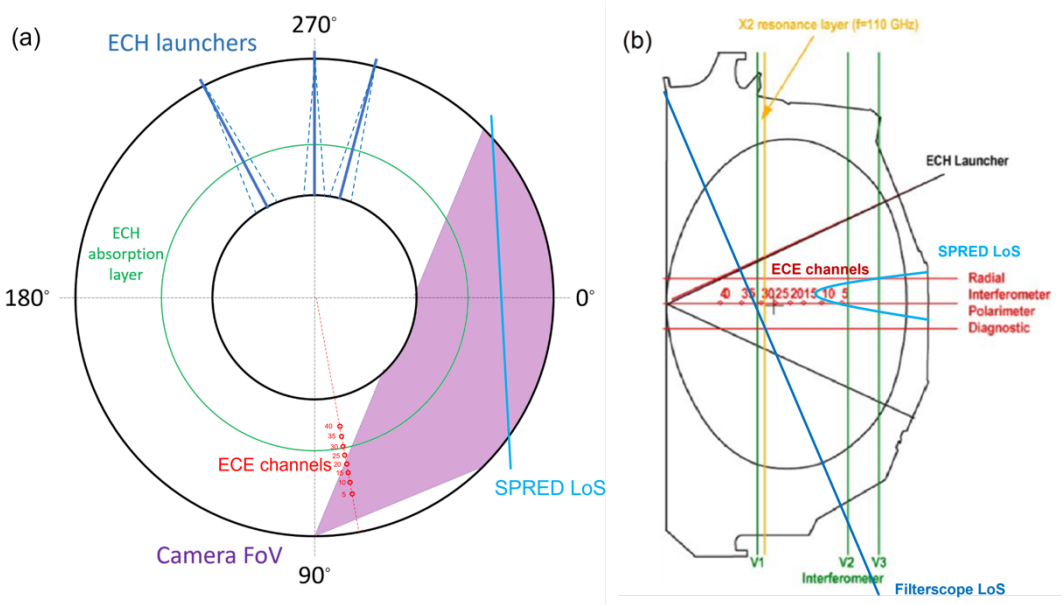

Figure 2: Overview of the DIII-D tokamak showing the EC launcher toroidal location and LoS of some of the essential diagnostics for the characterization of the EC pre-ionization process. (a) DIII-D top view showing the EC beams (blue solid lines) and the dashed blue lines show

the maximum toroidal EC injection angle possible (the poloidal injection angle was not varied in these experiments), X2 resonance layer location (light green line), some of the selected radial locations of the ECE channels (red circles), the LoS of the SPRED diagnostic (cyan line) and FoV of the fast-framing camera (purple cone) (see also Figure 4b). (b) Poloidal view of DIII-D showing the X2 resonance layer position (yellow line), injected and reflected EC beam path (black lines), the LoS of the three vertical chords of the CO_2 interferometer (dark green lines), the ECE channels (red diamonds), the LoS of the filterscope diagnostic showing only chord number 11 (blue line) used during these experiments, the LoS of the SPRED diagnostic (cyan line) and three radial chords of the radial interferometer polarimeter diagnostic (red lines). The plasma boundary is denoted by the black oval shape.

3. Characterization of pre-ionized plasma

An example of the typical evolution of various parameters that can be used to characterize the ECH pre-ionization process is shown in Figure 3a, including the calibrated injected EC power (P_{ECH}) since it plays a significant role in the creation of the pre-ionized plasma. As discussed in Section 2, there is only a limited set of diagnostics that can be used to quantify the pre-ionized plasma parameters. These include the following quantities: (1) maximum I_{P}, (2) maximum line-integrated plasma density ($n_{\mathrm{e}}^{\mathrm{max}}$), (3) time of the D_α emission peak with respect to the start of the EC pulse ($t_{\mathrm{D}\alpha}^{\mathrm{peak}}$), (4) maximum T_{e} of the pre-ionized plasma ($T_{\mathrm{e}}^{\mathrm{max}}$) and (5) the time it takes to reach the maximum pre-ionized n_{e} and T_{e}.

A very small, but measurable I_{P} ~ 5-7 kA, is also observed in the EC pre-ionization phase during these and previous experiments [3, 4]. The $t_{\mathrm{D}\alpha}^{\mathrm{peak}}$ is determined from the D_α emission measurements obtained from the line of sight of the filterscope diagnostic, which passes through the resonance layer location (see Figure 3d) and provides information about the degree of ionization of the neutral gas close to the resonance layer location during the EC pre-ionization process. The peaking of the D_α emission indicates at least 50% of the deuterium gas [2] is ionized within the FoV of the camera and is a reasonable definition for the timing of the local burn-through of the main species. As shown in Figure 3e, the value of $n_{\mathrm{e}}^{\mathrm{max}}$ is ~10^{19} m^{-2} for P_{ECH} = 1.4 MW (obtained from the V1 interferometer chord). Note that the local electron density is too low for the plasma to be optically thick for EC waves. Hence, only a small fraction (roughly a few percent) of the ECH power is expected to be absorbed by the pre-plasma.

An indication of T_e is obtained from an ECE diagnostic channel (channel 25) close to, but not at, the ECH resonance layer location. Those ECE channels that measure at the ECH resonance are usually badly disturbed by the ECH injection and cannot be used, while those further away do not always register a signal because T_e is too low. In common with the absorbed power measurement, interpretation of these ECE signals must be made with care because the plasma is far from optically thick. This will be discussed further at the end of this section. As shown in Figure 3f, the measured T_{ECE} drops significantly as soon as the EC pulse is switched off. The time it takes to reach the maximum pre-ionized plasma n_e and T_e is usually of the order of few tens of ms.

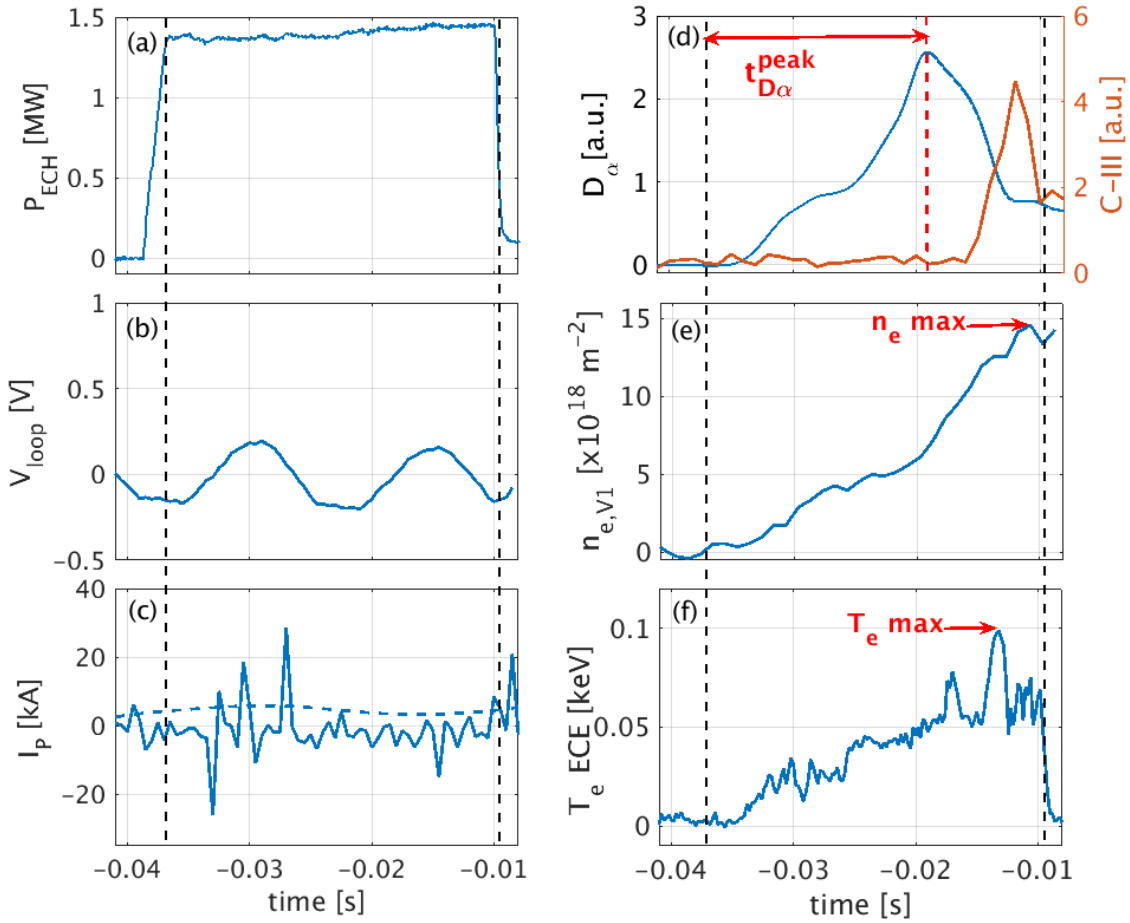

Figure 3: Example of characterization of the pre-ionized plasma during the EC pre-ionization phase. Evolution of (a) injected EC power, (b) applied V_{loop}, (c) measured I_P, (d) D_α emission measurement (blue line) obtained from the line of sight of the filterscope diagnostic, which passes through the region of the ECH resonance layer location and C-III emission measurement (red line) obtained from the SPRED diagnostic , (e) line-integrated density measurement from the V1 chord of the interferometer, and (f) T_{ECE} or ECE radiation temperature measured by the ECE diagnostic from the channel 25 (i.e. close to the ECH resonance). The dashed black lines

denote the EC pulse duration, and the red dashed line represents the time corresponding to the D_α emission peak.

As discussed in Section 2, the fast-framing camera has been used in these experiments to study the evolution of different stages of the EC pre-ionization process. Figure 4 shows the image obtained using the fast-framing camera a few ms after the EC injection is turned-on. The central column (Ohmic transformer) of DIII-D is located on the left-hand side of the image (x pixel: 0-100, $R \sim 1.1$ m), the outer wall is on the right-hand side (x pixel: 350-512, $R \sim 2.4$ m) and the EC X2 resonance layer location is at x pixel = 210, corresponding to $R = 1.52$ m. As can be seen in Figure 4, the toroidal ring formation occurs already 4 ms after the EC injection is switched on and connects the first (upper, i.e. at y pixel: 260) intersection of the EC beam with the X2 resonance layer. It should be noted that, as mentioned previously, the FoV of the fast-framing camera does not view the toroidal location where the EC beam is injected (see Figure 2a), thus the plasma must already extend toroidally and has formed a toroidal plasma tube. The EC beam is reflected from the central column and crosses the resonance again at approximately y pixel 150, but at this moment in time a second toroidal tube is not yet visible.

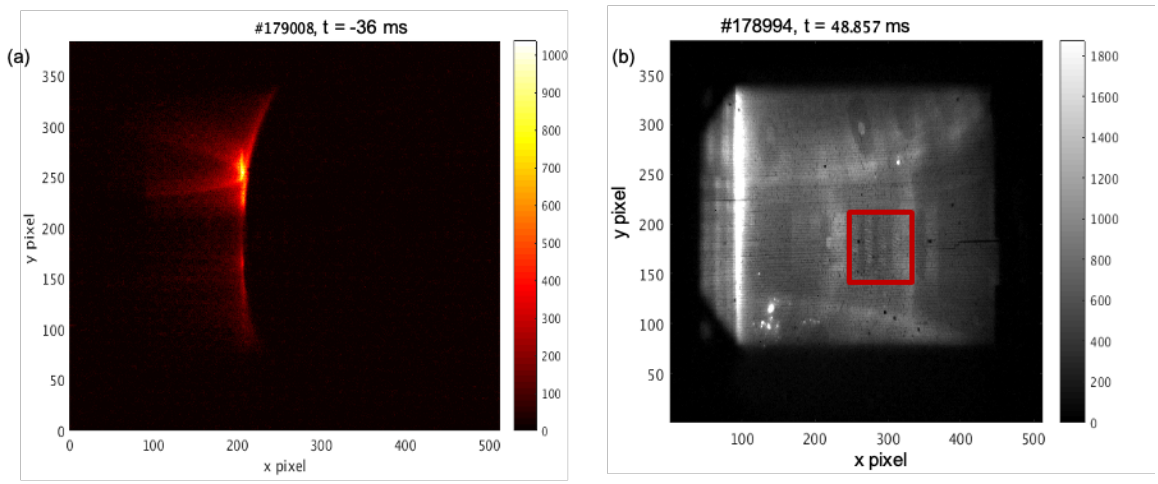

Figure 4: a) The image obtained using the fast-framing camera 4 ms after the EC injection was turned-on for shot 179008 (t = -36 ms). The main emission is at the location of the EC resonance, while the brightest light is emitted from the poloidal region where the first pass of the EC beam intersects with the EC resonance. The horizontal axis shows the number of pixels (x-pixel), linked to radial positions of the viewing lines, while the y-pixels are linked to the vertical positions. b) The image obtained for shot 178994 in the presence of a hot plasma, allows some of the DIII-D structures in view of the camera to be visible. On the left (at x-pixel = 100) is the central column, while the toroidal limiter structures and fast wave-antenna (highlighted by the red square) are also visible. See also Figure 2a.

Figure 5 shows the evolution of the different phases of the EC pre-ionization process obtained using the fast-framing camera, specifically for a case with radial ECH injection. Figure 5a shows the temporal evolution of the intensity averaged over the region where the first pass of the injected EC beam at the X2 resonance layer occurs (denoted by the blue box in Figure 5c) and the region where the second pass of the reflected EC beam at the X2 resonance layer occurs (denoted by the red box in Figure 5c). Phase I and II of the EC pre-ionization process take place before t = -37 ms (i.e. within the first 3-4 ms after the EC injection is switched on). Phase III, which corresponds to the local burn-through of the main neutral gas and the impurities close to the X2 resonance layer takes longer and depends on the amount of injected ECH power. In this discharge, it takes place between t = -36 ms to t = -20 ms (Figure 5b – 5d), with the peak of the visible radiation reaching its maximum value at ~ -27 ms. For this example, the local burn-through in the first and second pass cases develop very similarly. The roll-over or peaking of the local D_α emission suggests that at these locations the local ionization fraction exceeds 50% and that T_e > 20 eV. There is also visible emission observed in between the crossings of the resonance. Phase IV of the EC pre-ionization phase corresponds to the radial expansion of the EC pre-ionized plasma from the resonance to the outer wall (Figure 5e and 5f). As is known from previous experiments [4], this expansion is asymmetric with respect to the EC resonance. More detail on the radial expansion of the pre-ionized plasma will be given later in this section.

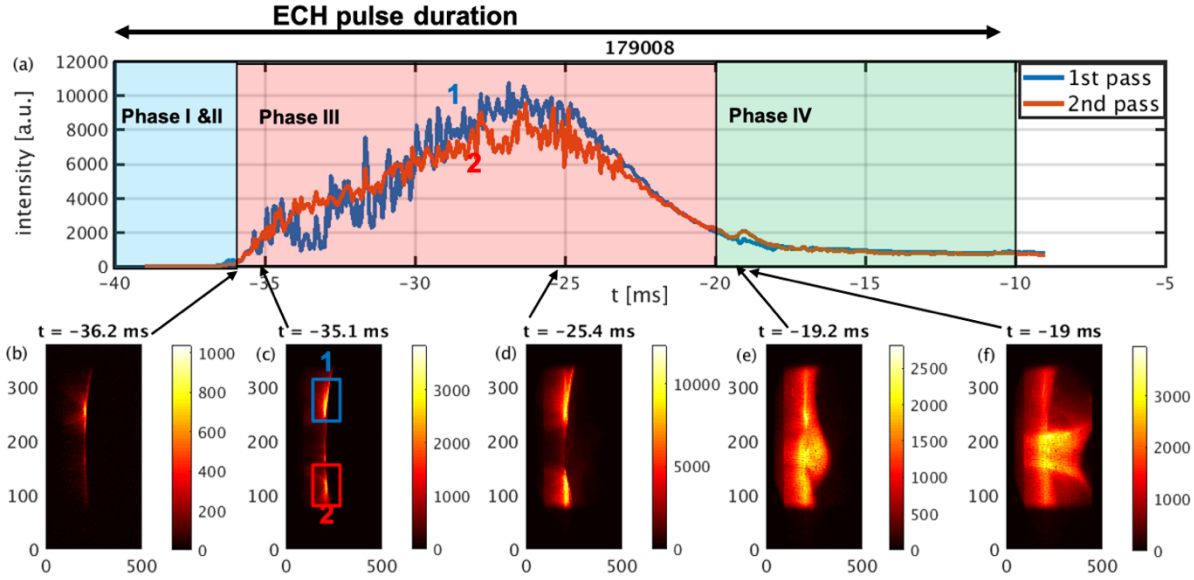

Figure 5: Evolution of the EC pre-ionization process obtained using the fast-framing camera for a radial EC injection case that uses P_{ECH} = 1.4 MW and a p_0 = 0.0025 Pa. (a) Temporal evolution of the intensity averaged over the region where the first and the second pass of the

EC beam at the X2 resonance layer occurs. (b)-(f) Images from the fast-framing camera taken at different times during the EC pre-ionization process. The blue and red boxes correspond to the region where the first pass and the second pass of the EC beam at the X2 resonance layer occur respectively.

A second example of the evolution of the different phases of the EC pre-ionization process, specifically for a tangential co-current EC injection case is shown in Figure 6. The phases I and II occur within the first 5 ms after the ECH is switched on, as shown in Figure 6a, and the phase III starts from t = -35 ms and lasts until -16 ms (Figure 6b – 6d). However, in contrast to the radial injection case, a difference is observed between the maximum values of the intensity averaged over the regions where the first and second passes of the EC beam intersect the X2 resonance layer (Figure 6a). Clearly the second pass is now less effective in heating the local plasma. Phase IV of the EC pre-ionization process starts at t = -15 ms onwards (Figures 6e and 6f). Comparison of the radial and tangential co-current EC injection cases (Figures 5 and 6) shows that there is a difference in the temporal evolution of the different phases of the EC pre-ionization process even though both the cases have the same P_{ECH} = 1.4 MW and p_0 = 0.0025 Pa. Phase IV, i.e. radial expansion of the pre-ionized plasma, is delayed in the case of tangential co-current EC injection compared to the radial injection case.

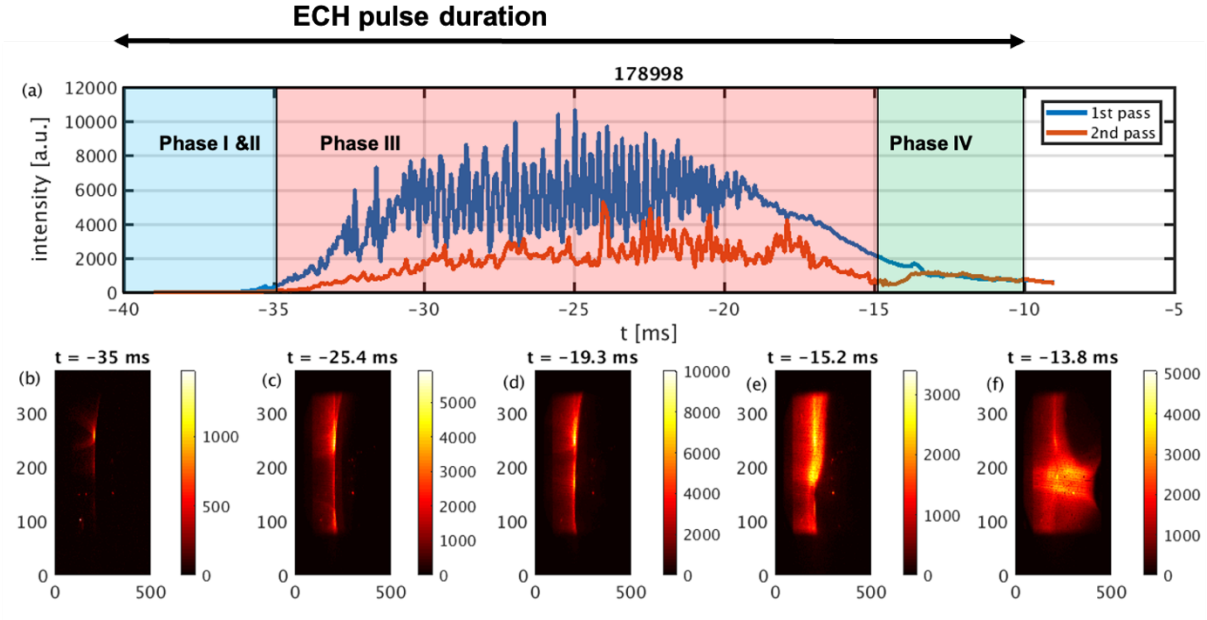

Figure 6: Evolution of the EC pre-ionization process obtained using the fast-framing camera for a tangential EC injection case with P_{ECH} = 1.4 MW and a prefill pressure of 0.0025 Pa. (a) Temporal evolution of the intensity averaged over the region where the first and the second

pass of the EC beam at the X2 resonance layer occurs. (b)-(f) Images from the fast-framing camera taken at different times during the EC pre-ionization process.

Parametric scans (in P_{ECH}, EC toroidal injection angle and prefill pressure) were performed to understand the influence of the various parameters on the EC pre-ionization process. Additional parameters, such as the value of the externally applied vertical magnetic field, the EC harmonic and time interval of the EC pulse being applied, have not been scanned during these experiments since some of this information is already available from detailed previous experiments [4, 5].

The effect of the different parameters on the EC pre-ionized plasma is characterized by using the following quantities: $n_{\mathrm{e}}^{\mathrm{max}}$, $t_{\mathrm{D}\alpha}^{\mathrm{peak}}$, $T_{\mathrm{ECE}}^{\mathrm{max}}$ and the time it takes to reach the maximum pre-ionized plasma density and temperature. Figure 7a shows the effect of the injected ECH power on the rate, $\mathrm{d}n_{\mathrm{e}}/\mathrm{d}t$ at which n_{e} increases during the pre-ionized plasma density rise phase (until the maximum density is reached) for both the radial and tangential EC toroidal injection angle. For the radial EC injection case, an increase in the injected ECH power results in a higher $\mathrm{d}n_{\mathrm{e}}/\mathrm{d}t$ for same p_0. A similar trend is observed for the tangential co-current EC injection case. Therefore, the higher the EC injected power results in a larger increase in the pre-plasma density rise rate close to the X2 resonance layer location.

Figure 7b shows $n_{\mathrm{e}}^{\mathrm{max}}$ as a function of P_{ECH} and a similar trend was observed for the $n_{\mathrm{e}}^{\mathrm{max}}$ close to the resonance layer, namely $n_{\mathrm{e}}^{\mathrm{max}}$ increases with the increase in P_{ECH}. It was also observed that there is a threshold in P_{ECH} below which no pre-plasma density is observed, and this value is different for different EC injection angles. The threshold values of P_{ECH} are 0.5 MW and 0.75 MW for the radial and tangential co-current injection cases respectively. At the same P_{ECH} and p_0, the radial EC injection resulted in a faster increase in the pre-plasma density compared to the tangential injection. Note that the threshold powers are significantly higher than that predicted for non-linear ionization by EC waves, as discussed in Section 1 [14]. But the latter is relevant to the process that initiates Phase I, while the threshold measured in these experiments and documented in Figure 7 concerns the build-up of a significant local plasma density (Phase III).

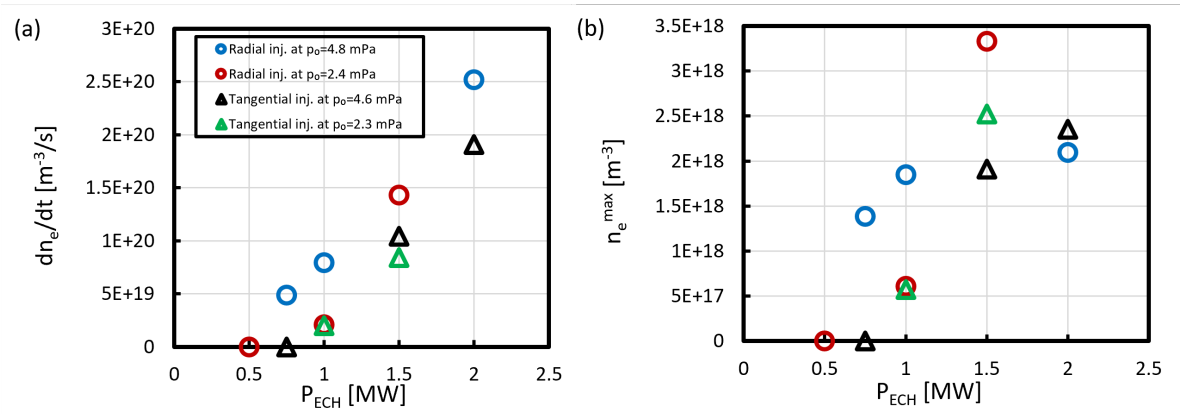

Figure 7: Effect of P_{ECH} on (a) the density increase rate during the pre-ionized plasma density rise phase, and (b) the maximum pre-ionized plasma density for both radial and tangential co-current EC injection angle. The circles denote the radial injection cases with the blue and red colours denoting the two different values of p_0. The triangles denote the tangential co-current cases with the green and black colours denoting the two different values p_0.

A rough estimate of the line-averaged density can be obtained by dividing the line-integrated densities by the vertical length of the observed pre-plasma along the X2 resonance, as shown in Figure 7. This length is $l \sim 4.68$ m and means that maximum line-averaged densities of 0.5-3 $\times$ 10^{18} m^{-3} are found in these experiments. Note that the obtained value of n_{e} with respect to p_0 is correlated with the degree of ionization achieved. Another way to characterize the increase of ionization rate is by analyzing the local D_α emission, in particular the time at which it peaks, $t_{\mathrm{D}\alpha}^{\mathrm{peak}}$ for both radial and tangential EC injection cases as shown in Figure 8. Faster ionization of the neutral gas is observed at higher ECH powers for both cases, and local burn-through is achieved earlier with higher ECH powers. It was also observed that at low P_{ECH} (< 0.75 MW), the local burn-through of the neutral gas is not possible within the 30 ms time interval of the EC pulse. The times of local burn-through (i.e. 5-10 ms) when applying sufficient EC power (i.e. approximately 1.5 MW) are comparable, but slightly slower than what is observed in ASDEX-Upgrade during similar experiments [3].

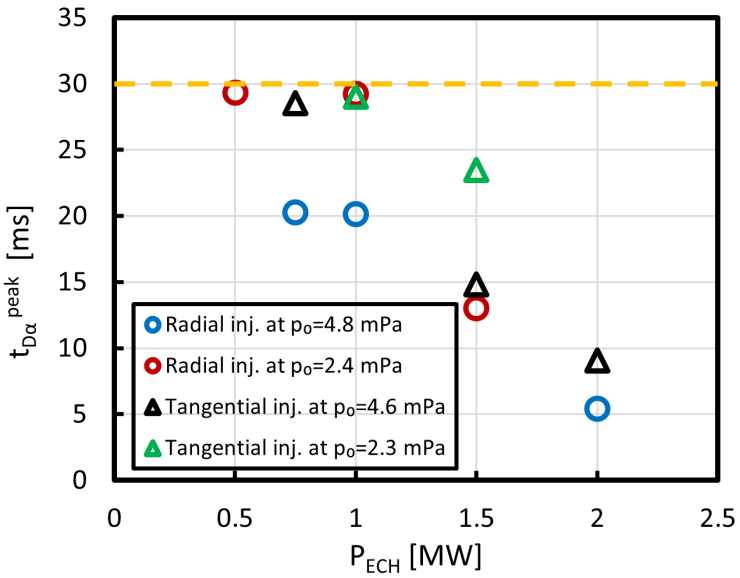

Figure 8: Effect of P_{ECH} on the $t_{\mathrm{D}\alpha}^{\mathrm{peak}}$ for both radial and tangential co-current EC injection. The circles denote the radial injection cases with the blue and red colours denoting the two different values of p_0. The triangles denote the tangential co-current cases with the green and black colours denoting the two different prefill values of p_0. The yellow dashed line corresponds to the 30 ms time interval of the EC pulse.

The effect of the variation of p_0 on the EC pre-ionization process was also studied during these experiments. This has been quantified in terms of both $\mathrm{d}n_{\mathrm{e}}/\mathrm{d}t$ and $t_{\mathrm{D}\alpha}^{\mathrm{peak}}$. Similar to earlier experiments [6], an optimum prefill pressure range is found for which the ECH pre-plasma formation is more efficient (i.e. a higher pre-plasma density is achieved), as shown in Figure 9. For the same P_{ECH} and EC injection angle, $\mathrm{d}n_{\mathrm{e}}/\mathrm{d}t$ decreases if the p_0 is either increased or decreased with respect to the optimum value. This means that if the pre-fill pressure is too low, the pre-plasma will not establish, while if it is too high it may take too long to develop a high enough density to be detected, or to create a local burn-through within the desired time. This is reminiscent of the range of p_0 for which an inductively driven discharge would establish if a voltage is applied [2].

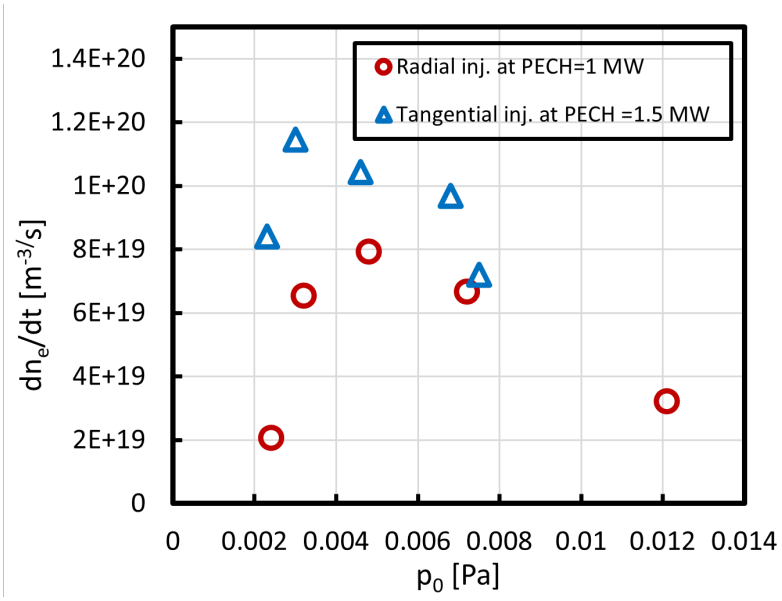

Figure 9: Effect of p_0 on $\mathrm{d}n_\mathrm{e}/\mathrm{d}t$ during the EC pre-ionization phase. The triangles denote the tangential co-current injection and the circles the radial injection case. Note that different levels of P_ECH are applied for the radial and tangential injection experiments.

Figure 10 shows the effect of p_0 on $t_{\mathrm{D}\alpha}^{\mathrm{peak}}$ for different EC injection angles. It was observed that too high or too low a value of p_0 results in slower ionization of the neutral gas and, therefore, local burn-through of the D_α was not observed during the 30 ms time interval of the EC pulse for such conditions. An optimum p_0 range between 0.002 to 0.005 Pa, was found where an increase in p_0 resulted in decrease of D_α peak timing. A higher value than the optimum of ~ 0.005 Pa slows down the ionization of the neutral gas (i.e. a slower increase in the local n_e), and results in a later D_α peak and no burn-through.

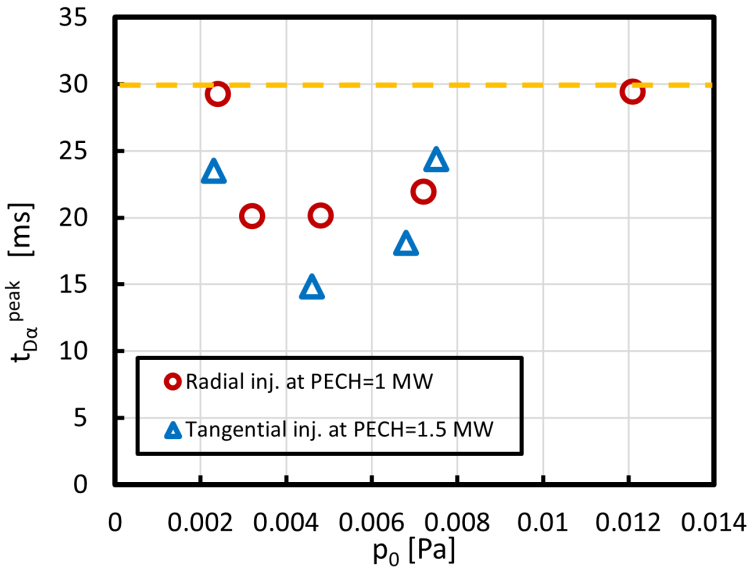

Figure 10: Effect of the p_0 on $t_{D\alpha}^{peak}$ for both radial and tangential co-current EC injection. The triangles denote the tangential co-current injection and the circles the radial injection case. The yellow dashed line corresponds to the 30 ms time interval of the EC pulse. Note that different ECH power levels are applied for the radial and tangential injection experiments.

Another parameter that can be used to characterize the pre-ionized plasma is the local T_{ECE} obtained from the channel 25 of the ECE diagnostic, which is located close to the resonance layer location. Figure 11 shows the effect of P_{ECH} on the T_{ECE}^{max} showing that the increase in the injected ECH power results in a higher T_{ECE}^{max} for both the radial and tangential co-current EC injection cases. It was also observed that the radial EC injection case results in a higher T_{ECE}^{max} compared to the tangential one even for the same p_0 and P_{ECH} values. As noted above, the interpretation of the value of T_{ECE} should be approached with care since the pre-plasmas are far from optically thick and, thus, T_{ECE} cannot be reliably related to T_e. Nevertheless, the range of temperatures and their asymmetry are also consistent with early experiments on EC pre-plasmas in DIII-D [4, 5], and consistent with the observation that these pre-plasmas achieve local burn-through for higher powers.

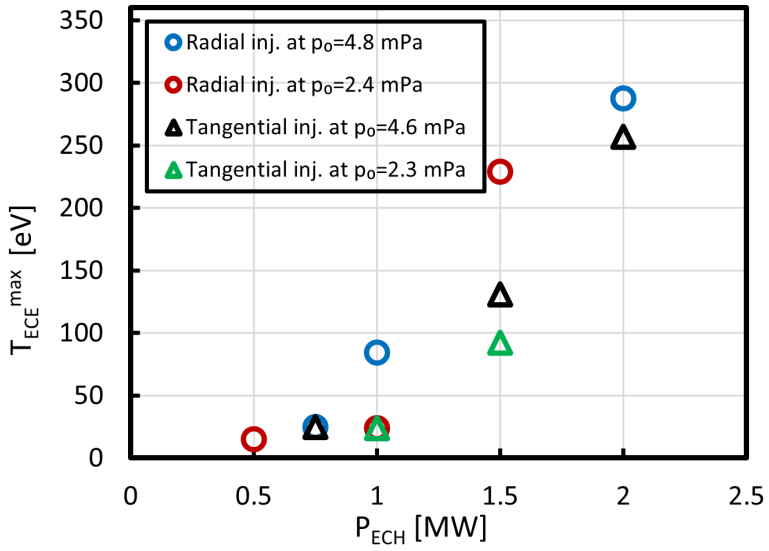

Figure 11: Effect of P_{ECH} on $T_{\mathrm{ECE}}^{\mathrm{max}}$ for both radial and tangential co-current EC injection. The circles denote the radial injection cases with the blue and red colours denoting the two different values of p_0. The triangles denote the tangential co-current cases with the green and black colours denoting the two different p_0 values.

Lastly, the characterization of phase IV of the EC pre-ionization process was also performed based on the time, $t_{\mathrm{expansion}}$, it takes for the start of the radial expansion to take place with respect to the switch on of the ECH injection (i.e. the time for the pre-plasma to expand from the X2 resonance layer to the outer wall, as shown in Figure 5f). It was observed that the radial expansion occurs earlier at higher P_{ECH} for both the radial and tangential co-current injection cases (Figure 12). If P_{ECH} is too low, the expansion may not take place within the duration of the EC pulse (i.e. 30 ms for these experiments). The additional power threshold to achieve expansion is higher (>1 MW) than the one noted above for the pre-plasma to locally burn-through. The radial expansion occurs only after the local burn-through of the neutral gas has been completed (i.e. after the completion of phase III). The exact mechanism that drives the asymmetric radial expansion of the plasma remains an active area of study [4, 5]. In the experiments here, it was noted that the radial expansion of the pre-ionized plasma results in interaction with the outer wall, bringing in impurities. The latter will have, as will be seen in the next section, a detrimental effect on the plasma initiation induced by the V_{loop}.

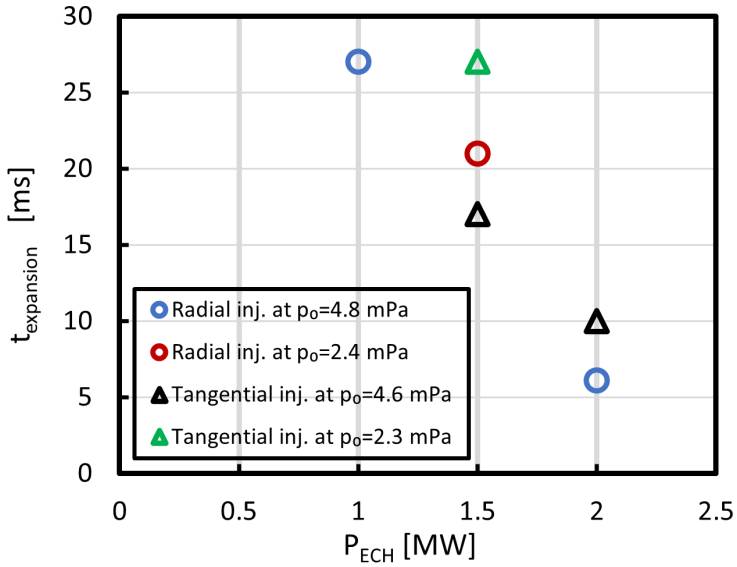

Figure 12: Effect of the P_{ECH} on $t_{\mathrm{expansion}}$ for both radial and tangential co-current EC injection. The circles denote the radial injection cases, with the blue and red colours denoting the two different values of p_0. The triangles denote the tangential co-current cases with the green and black colours denoting the two different p_0 values.

4. Characterization of the effect of the pre-plasma on the V_{loop} induced plasma

The next step in the study is to investigate how the EC pre-ionized plasma affects the V_{loop} plasma initiation process. The two processes were separated by switching-off the EC injection just before the application of the V_{loop} at t = - 9 ms (see Section 2 and Figure 1). The V_{loop} is feedback controlled in all of these experiments and pre-programmed so that its value reaches a maximum value of 4-4.5 V at $t \sim 5$ ms, which corresponds to a toroidal electric field of E_Φ = 0.4 V/m in the centre of DIII-D. This value of E_Φ is lower than is usually applied at DIII-D and chosen because it is closer to the value that is envisaged for ITER plasma initiation (E_Φ = 0.3 V/m). Moreover, at this lower value of E_Φ, the Ohmic plasma initiation process is more fragile, hence the positive effect of the EC either by pre-ionization or by burn-through assist, is more easily noticeable.

In these experiments the V_{loop} remained unchanged while studying the differences in the plasma initiation process, either due to the creation of an EC pre-plasma (EC injection applied prior to the application of a V_{loop}) or by applying EC to assist the burn-through (EC injection applied during the application of a V_{loop}). The experiments were carried out on two separate days, one set in July 2019 (Day-1) and the second in September 2020 (Day-2). Hence, differences in the vacuum and wall conditions between these days can affect the comparison

of these two data sets. Furthermore, the availability of diagnostics was not the same on both experimental days.

A successful plasma initiation process can be defined as the discharge being able to achieve burn-through of the impurities and plasma current ramp up to I_P = 100 kA. It was observed that on these two experimental days the purely Ohmic plasma start-up (i.e. neither an EC pre-plasma nor the use of EC for burn-through assist) at this low value of $V_{loop,}$ was not successful.

A number of typical plasma initiation parameters can be used to quantify the behaviour of both successful and failed plasma initiation cases. Figure 13 shows the measurements that were used for this purpose. These include the V_{loop}, the measured I_P, the D_α emission from the filterscope diagnostic, the C-III emission from the SPRED diagnostic and the measured line-integrated n_e obtained from the V1 chord of the interferometer. From these one can derive a number of quantities such as: (1) time of the D_α emission peak with respect to the start of the V_{loop} application ($\Delta t_{D\alpha}$) indicating the speed at which the early ionization process develops, (2) the average rate of change in plasma current (dI_P/dt), or as used here for easier characterization, determined through the time needed for the I_P to reach 50 kA, and (3) the ratio of the maximum value of the C-III emission peak to the plasma density at the time of the C-III peak ($CIII^{max}/n_e$), as a measure of the carbon content. It should be noted that value of I_P = 50 kA corresponds roughly to the current needed to form closed magnetic flux surfaces during the DIII-D plasma initiation process.

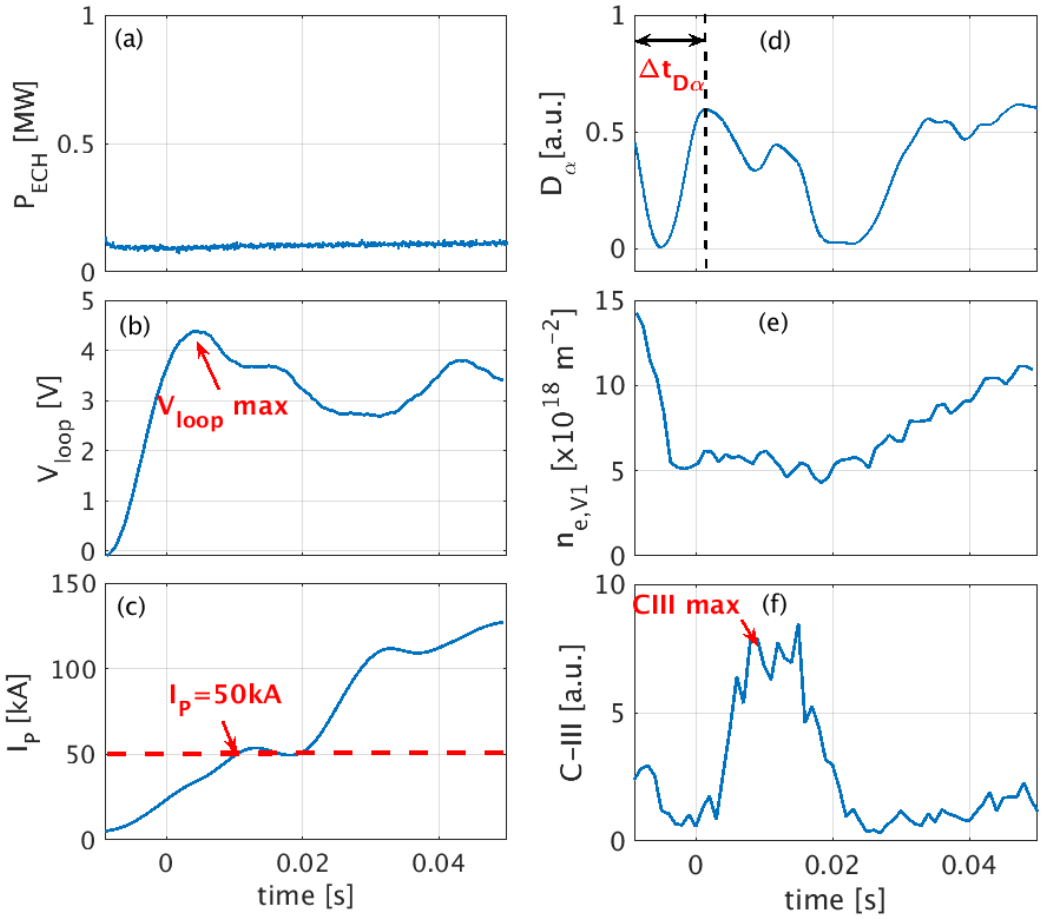

Figure 13: Example of characterization of the effect of the pre-ionized plasma on the V_{loop} induced plasma initiation process. Evolution of (a) P_{ECH}, (b) applied V_{loop}, (c) measured I_{P}, (d) D_{α} emission measurement obtained from the LoS of the filterscope diagnostic, (e) line-integrated density measurement from the V1 chord of the interferometer, and (f) C-III emission measurement from the SPRED diagnostic. The dashed black line denotes the time corresponding to the D_{α} emission peak and the dashed red line denotes the I_{P} = 50 kA value.

It was found that a higher $n_{\mathrm{e}}^{\mathrm{max}}$ results in a shorter $\Delta t_{\mathrm{D}\alpha}$ (thus faster ionization of the neutral gas) during the V_{loop} induced plasma initiation process, as shown in Figure 14a, for data taken on Day-1 of the experiments (red squares). Thus, the higher the pre-plasma n_{e}, the more the prefill gas is ionized during the EC pre-ionization process, and the easier it is to start-up (~10-12 ms) than the $\Delta t_{\mathrm{D}\alpha}$ ~ 22 ms found for the Ohmic start-up (black square) for high pre-ionized densities. Interestingly, when EC is used during the V_{loop} induced plasma initiation (to assist the burn-through phase) the time for the D_{α} to peak (blue squares in Figure 14a) is only slightly shorter than what is found for Ohmic plasma initiation.

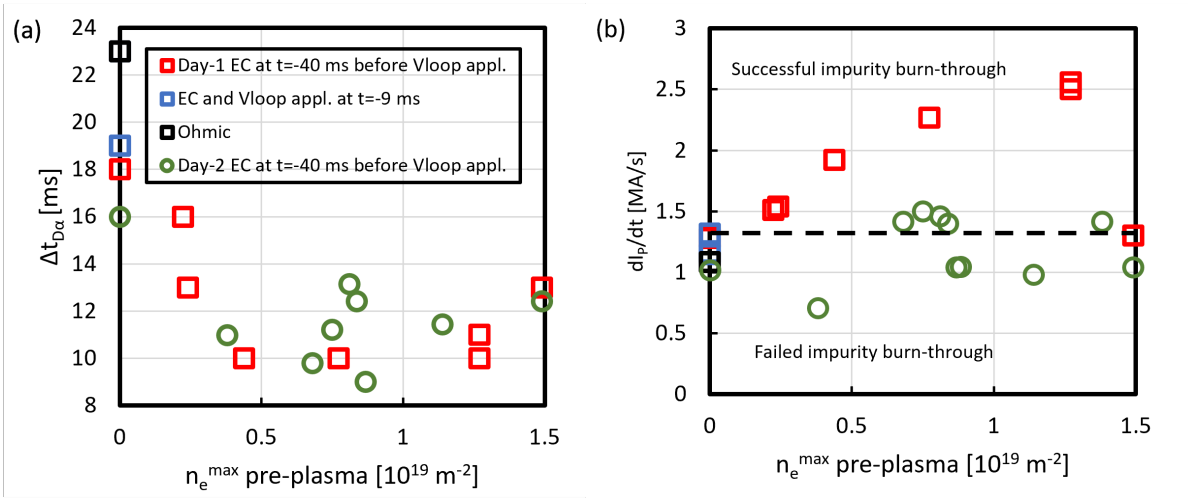

Figure 14: Effect of the pre-ionized plasma density on (a) $\Delta t_{\mathrm{D}\alpha}$ and (b) $\mathrm{d}I_{\mathrm{P}}/\mathrm{d}t$ for Day-1 and Day-2 of the EC pre-ionized plasma experiments. The red squares denote the shots having the EC pre-ionized plasma formation, the black square is the pure Ohmic case, and the blue squares denote the cases where V_{loop} and ECH beam were applied together for Day-1. The green circles denote the shots having EC pre-ionized plasma formation for Day-2. Please note that some of these cases, especially the Ohmic case, are non-successful plasma initiations.

Next it was observed that, in general, a pre-ionized plasma with a higher n_{e} results in a faster increase of I_{P} during the V_{loop} induced plasma initiation process as shown in Figure 14b. This suggests that a higher pre-plasma density allows the plasma temperature to increase faster during the V_{loop} induced plasma initiation, thus resulting in a lower resistance and a faster current rise. There is, however, a case on Day-1 that breaks this trend. This is the case with the highest achieved n_{e} during the pre-plasma, created with high power ECH (P_{ECH} = 1.4 MW radial injection). The development of this pre-plasma was such that the plasma expanded rapidly (Phase IV as discussed in Section 3) resulting in early, extensive plasma-wall interaction, during the pre-plasma phase, prior to the application of V_{loop}. It will be shown later that this resulted in a larger carbon concentration during the V_{loop} induced plasma initiation stage, which is detrimental to increasing I_{P} as shown in Figure 15. Clearly, too fast an expansion and plasma-wall interaction during the pre-plasma phase has a degrading effect on the V_{loop} induced plasma formation.

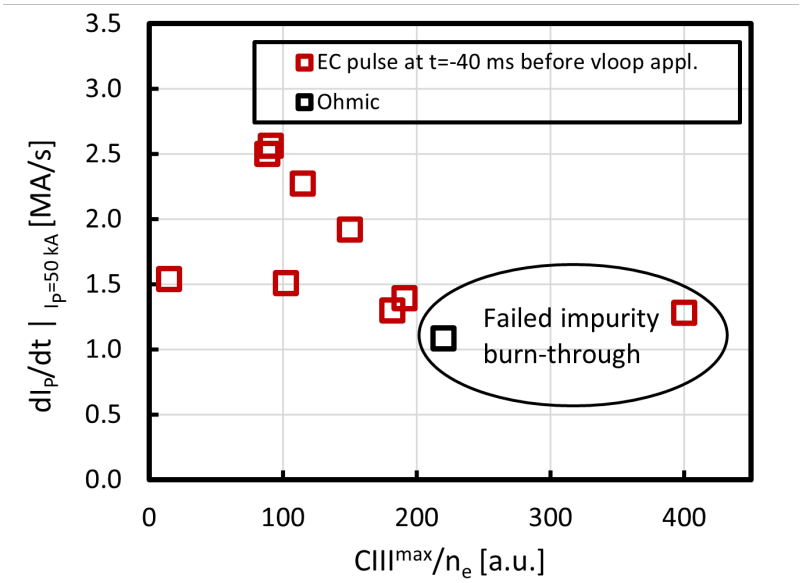

Figure 15: Effect of the impurity concentration ($\mathrm{CIII}^{\mathrm{max}}/n_{\mathrm{e}}$) on $\mathrm{d}I_{\mathrm{P}}/\mathrm{d}t$ during the V_{loop} induced plasma initiation process for the Day-1 of the EC pre-ionized plasma experiments. The red squares are the cases with the EC pre-ionzation process and the black square is the pure Ohmic case.

The studies were repeated during the second day of experiments (Day-2). The results obtained on the effect of the EC pre-ionized plasma on the $\Delta t_{\mathrm{D}\alpha}$ and the $\mathrm{d}I_{\mathrm{P}}/\mathrm{d}t$ are shown in Figure 14a and 14b (green circles), respectively. The same trend was observed for the $\Delta t_{\mathrm{D}\alpha}$ during the Day-2 experiments (green circles in Figure 14a) compared to the Day-1 experiments (red squares in Figure 14a). However, the nice trend found on Day-1 for $\mathrm{d}I_{\mathrm{P}}/\mathrm{d}t$ is not visible in the discharges of Day-2. The current ramp-rate for all cases on Day-2 was significantly reduced compared to what was found for Day-1, even though similar pre-plasma densities were observed (Figure 14b). It is likely that this is due to an increased resistance, a lower temperature and likely a larger impurity content for the Day-2 experiments. The reason for this difference in behaviour could be due to different wall or vacuum conditions of the DIII-D tokamak. For the Day-1 experiments, the vacuum vessel pressure was 9.7×10^{-6} Pa and the most recent baking and boronization was done 12 days before whereas for the Day-2, the vacuum vessel pressure was 2.4×10^{-5} Pa and most recent baking and boronization was done 12 days before. The difference in wall conditions clearly impacted the V_{loop} induced plasma initiation. It is however noteworthy that such differences between Day-1 and Day-2 experiments were not observed when characterizing the pre-plasma, as shown in Section 3. Thus, as long as the pre-ionized plasma remains small and does not expand up to the wall, it is not strongly affected by

the machine conditions. Moreover, the very early stages of the V_{loop} induced plasma formation, up to the time the D_α peaks, seems also unaffected (as shown in Figure 14a). It is assumed that machine conditions only changed the further development of the density and impurity content and eventually the plasma burn-through phase.

Figure 16 shows that there is a much larger variation in the density at the time of the burn-through phase (i.e., the line-integrated density at the time of the D_α peak during the V_{loop} induced plasma initiation), during Day-2 than for the Day-1 experiments. The difference in density might be caused by a difference in low-Z impurity content, but also outgassing of main-species from plasma-facing components during the plasma initiation process. For Day-2, the shots with lower n_{e} during burn-through phase resulted in higher $\mathrm{d}I_{\mathrm{P}}/\mathrm{d}t$ and successful V_{loop} induced plasma initiation. The shots with higher line-integrated density during burn-through phase resulted in lower $\mathrm{d}I_{\mathrm{P}}/\mathrm{d}t$ and failed plasma initiation. Higher levels of outgassing would also lead to the observed higher n_{e}, lower T_{e}, higher resistance and thus lower $\mathrm{d}I_{\mathrm{P}}/\mathrm{d}t$. Clearly, one indicator on the quality of the V_{loop} induced plasma initiation process, the time for D_α to peak, is affected in a different way compared to the other indicator, $\mathrm{d}I_{\mathrm{P}}/\mathrm{d}t$. This comparison between the experiments in the two days also shows how important the choice of these two indicators to characterize plasma initiation is.

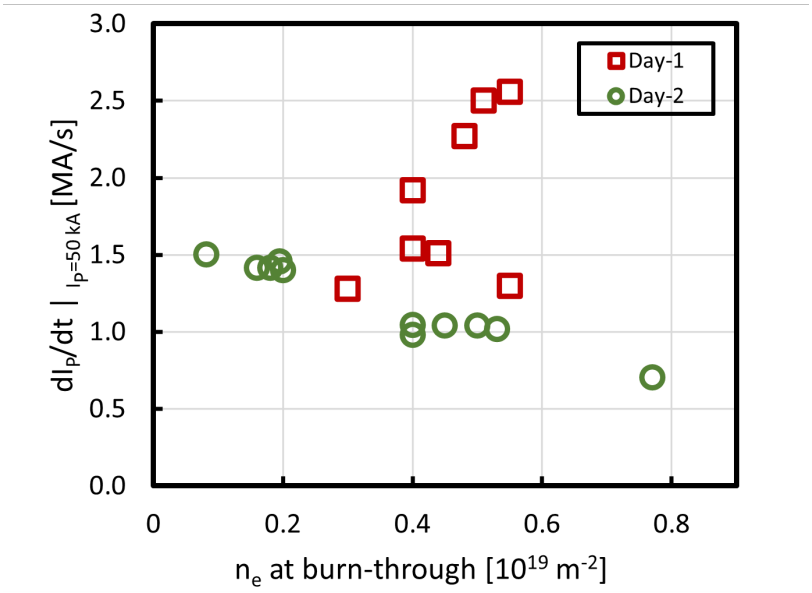

Figure 16: Comparison of the effect of the line-integrated density at the time of the burn-through phase on $\mathrm{d}I_{\mathrm{P}}/\mathrm{d}t$ for Day-1 and Day-2 of the EC pre-ionized plasma experiments. The red squares denote the shots having the EC pre-ionized plasma formation for Day-1, and the green circles denote the shots having the EC pre-ionized plasma formation for Day-2.

5. Extrapolation to ITER

The extrapolation of the DIII-D results to ITER is not a straightforward matter for a number of reasons. As shown above, there are several different factors that are relevant, such as the ECH power threshold to achieve ionization [14] and furthermore the ECH power and/or time scale to create a high-quality pre-plasma with sufficient ionization. The first is theoretically well understood and it can be shown that, according to ref. [14], that a X2 ITER ECH beam of 500 kW will be able to increase the electron energy into the range where the ionization cross-section is maximum (i.e. 60 eV). Thus, the 1MW ECH beams at ITER will create ionization at the locations where the ECH beam crosses the resonance. For FP it is planned to inject ECH from one upper launcher in ITER and allows it to reflect from the inner wall back through the plasma, which is a very similar scheme to what was used in the DIII-D experiments reported here. Thus, one expects ionization near the location where the ECH beam first passes the resonance and, at a level, less ionization effect at the 2nd pass location. The question is whether these local ionizations are sufficient to support plasma initiation.

As shown by the experiments discussed here, different levels of P_{ECH} are required at the different phases (I - IV) of the pre-plasma and, presumably, the burn through. For example, sufficient power is needed to create a higher level of ionization in the relevant breakdown area. The scaling of this second criterion is, however, complicated. This extrapolation depends more on the exact geometry of the injection of the ECH, not only on the toroidal angle, which is a well-known relevant parameter, but also on how these beams pass through the vessel and are reflected from in-vessel components. Specifically, for ITER First Plasma operation, the EC beams will pass from the launcher through the very upper part of the vessel to be reflected via a set of mirrors on to the inner vessel wall, such that they pass once through the breakdown region, into a beam dump on the low field side mid-plane. For subsequent operational stages, once the blanket shield blocks and first wall are installed, multi-pass reflections will occur. Furthermore, the separation between the pre-plasma and the V_{loop} voltage-induced plasma initiation process in the range achieved in this experiment is not possible at ITER (and other devices, typically with superconducting coils). In ITER the electric field builds up slowly, over a timescale of several hundred milliseconds, and ECH assist will be applied jointly with the electric field. Exact extrapolation of experimental results is thus only possible if the experiments are repeated, in the same manner and with the same experimental criteria, but in a device of different size than DIII-D including a scan of the overlap between ECH and electric

field application. Nevertheless, it is possible to disentangle from the DIII-D experiments some of the most important features and discuss what can be expected for ITER.

For the ECH pre-plasma formation to affect the ITER plasma initiation, the process (of ionization) needs to be faster than what is achieved by the loop voltage. For the applied low peak electric field of 0.4 V/m, the Ohmic ionization process in DIII-D lasts about 15-23 ms (see Figure 14 in Section 4, in ref [1]). This time scale can be compared with the duration to achieve the same effect solely by ECH, which can be significantly faster for the highest ECH powers used in these experiments (down to 5 ms see Figure 8). This means that when the ECH pre-plasma formation process takes place simultaneously with the application of the loop voltage in DIII-D, the ECH generated process can be more significant than the ohmic processes, especially in the very early stages (before the time when the D_α peaks) when I_P is still low, if sufficient power is applied.

The experiments suggest that the key process, for the formation of the pre-plasma and its further ionization, is the heating of the plasma that surrounds the EC resonance. The net heating is obtained from the balance between the absorbed EC power (which is linearly dependent on n_e and T_e [2]), and energy losses, either by direct particle losses (there are open field lines, and the charged particles are prone to drifts) or energy losses due to ionization of neutrals, impurity line-emission or bremsstrahlung, similar to start up with induction [7]. As shown in these DIII-D experiments, this depends on p_0, (since the neutrals from the area outside the plasma will enter and be ionized in it), and on the heating of the pre-plasma. The scaling parameter in this process is the volume of the pre-plasma, which is considered to be a toroidal ring, with a radius equal to the EC resonance location, and with width and height that depends on the vertical part of the EC resonance that is affected by the EC beams. This last point strongly depends on how the geometry of the EC beams and their reflections cross the resonance at various vertical locations but as shown experimentally, it is also affected by the applied vertical field [3, 5, 6]. ITER will employ only single pass ECH in the breakdown region for FP operation, but the 7 ECH beams cross the resonance at different vertical locations, thus increasing the affected volume. One could estimate the EC pre-plasma volume to scale roughly as $R_0 \times a \sim R_0^2$ (where R_0 is the device major radius and the minor radius). This would suggest that to achieve similar conditions in ITER (R_0 = 6.2 m) as have been obtained in DIII-D (R_0 = 1.7 m), the minimum EC power of 0.5 MW found in DIII-D to obtain EC pre-ionization (i.e., Phases I and II of the EC pre-ionization process) would scale to a minimum power of roughly 6.5 MW for ITER. Similarly, the EC power threshold of 1 MW found in DIII-D, for a high-

quality pre-plasma (i.e., Phase III of the EC pre-ionization process), which forms within the time-scale of V_{loop} induced plasma initiation, would scale to a power of roughly 12 MW for ITER. It should be noted that this EC power threshold value is based on the use of X2 ECH, but O1 ECH is known to be more efficient to pre-ionize and heat the plasma [14]. Therefore, likely for O1 ECH less power will be required. However, since the main objective of ITER FP operation is the demonstration of plasma initiation only and not the formation of a full plasma discharge, this second and higher threshold may be of less relevance for the FP campaign. The exact power threshold may be affected by details of the ECH injection scheme that may differ from device to device. The scaling of this threshold to ITER would benefit from further similar experiments at devices smaller or larger than DIII-D.

6. Conclusions

The experiments reported in this paper build on a strong basis of earlier studies on ECH assisted plasma initiation done in DIII-D and other devices [3, 6, 7, 8, 9]. These EC pre-ionization experiments have shown that the pre-ionized plasma can have a significant impact on the subsequent V_{loop} induced plasma initiation process. Therefore, in order to quantify the effect of the ECH pre-plasma, a series of parameters have been determined that characterize the plasma initiation process. It is found that the pre-plasma characteristics are influenced by several parameters, such as the pre-fill pressure and the ECH injection angle (radial or tangential). However, the main observation is that sufficient ECH power must be injected to obtain a measurable effect on the V_{loop} induced plasma current ramp-up in DIII-D and this minimum power is of the order of 1MW. This threshold power is higher than the expected EC power levels needed to create ionization, based on ref. [14], which is of the order of 100 kW (see Section 1). This last criterion [14] predicts the required power levels, for the initial ionization to form near the resonance, but it is found that more power is needed to form a toroidally expanded plasma, with a sufficient degree of ionization. At higher power levels, (i.e. >1 MW) a local burn-through of the neutral gas is observed, suggesting that the pre-plasma ionization fraction locally exceeds 50%. A further critical parameter is the time needed to achieve a high-quality pre-plasma (i.e. high electron density and high ionization fraction). If it forms too slowly, then the duration of the DIII-D pre-plasma stage may be too short to achieve the required quality. Moreover, if ECH pre-ionization is combined with the application of the V_{loop}, its effect may develop on a longer time-scale (i.e. the time for D_α to peak) than the expected duration of the V_{loop} induced breakdown.

Many of the aspects of the pre-plasma formation are similar to the formation of ECWC plasmas, such as, the asymmetric radial expansion of the pre-ionized plasma appears to be similar to the cases observed in TCV for the ECWC plasmas [15]. The aim of ECWC plasmas is, however, to condition the plasma-facing components, hence these plasmas need only reach phase IV (see Section 3) in which the pre-plasma is fully expanded into the vessel. It has been shown here that the pre-plasmas created with the highest ECH powers in DIII-D expand very quickly and that the resulting plasma-wall interaction brings in impurities, which for plasma initiation has a detrimental effect. Hence, the optimum power levels to assist the pre-ionization for plasma initiation will have to be lower than those used for ECWC.

The observed power thresholds required to create high quality pre-plasmas in DIII-D and the time-scales at which they form, can be roughly extrapolated to ITER. However, the error bar on the estimated power is large and further careful analysis and further comparison with EC assisted breakdown in other devices is needed to obtain a more accurate estimate of the required EC powers for ITER pre-ionization assist.

Disclaimer

The views and opinions expressed herein do not necessarily reflect those of the ITER Organization.

Acknowledgment

This material is based upon work supported by the U.S. Department of Energy, Office of Science, Office of Fusion Energy Sciences, using the DIII-D National Fusion Facility, a DOE Office of Science user facility, under Award(s) DE-FC02-04ER54698, DE-AC02-09CH11466,

DE-FG02-04ER54761, DE-SC0019004, DE-FG02-07ER54917, DE-AC05-00OR22725 and DE-AC52-07NA27344.

References

[1] B. Lloyd et al 1991 Nucl. Fusion **31** 2031
https://doi.org/10.1088/0029-5515/31/11/001

[2] P.C. de Vries and Y. Gribov 2019 Nucl. Fusion **59** 096043
https://doi.org/10.1088/1741-4326/ab2ef4

[3] J. Stober et al 2011 Nucl. Fusion **51** 083031
https://doi.org/10.1088/0029-5515/51/8/083031

[4] G.L. Jackson et al 2007 Nucl. Fusion **47** 257
https://doi.org/10.1088/0029-5515/47/4/003

[5] G.L. Jackson et al 2010 Phys. Plasmas **17** 056116
https://doi.org/10.1063/1.3374242

[6] G.L. Jackson et al 2011 Nucl. Fusion **51** 083015
https://doi.org/10.1088/0029-5515/51/8/083015

[7] B. Lloyd et al 1996 Plasma Phys. Control. Fusion **38** 1627
https://doi.org/10.1088/0741-3335/38/9/007

[8] R. Yoshino et al 1997 Plasma Phys. Control. Fusion **39** 205
https://doi.org/10.1088/0741-3335/39/1/012

[9] Y.S. Bae et al 2009 Nucl. Fusion **49** 022001
https://doi.org/10.1088/0029-5515/49/2/022001

[10] Max E Fenstermacher et al 2021 Nucl. Fusion in press
https://doi.org/10.1088/1741-4326/ac2ff2

[11] D. Ricci et al 2016 Proc. of the 43rd EPS conference on Plasma Physics O5.130
http://ocs.ciemat.es/EPS2016PAP/pdf/O5.130.pdf

[12] H.T. Kim et al 2013 Plasma Phys. Control. Fusion **55** 124032
https://doi.org/10.1088/0741-3335/55/12/124032

[13] D. Ricci et al 2019 Proc. of the 46th EPS conference on Plasma Physics O5.103
http://ocs.ciemat.es/EPS2019PAP/pdf/O5.103.pdf

[14] D. Farina 2018 Nucl. Fusion **58** 066012
https://doi.org/10.1088/1741-4326/aabaa7

[15] T. Wauters et al 2020 Plasma Phys. Control. Fusion **62** 034002
https://doi.org/10.1088/1361-6587/ab5ad0

[16] G. Haas and H-S. Bosch 1998 Vacuum **51** 39
https://doi.org/10.1016/S0042-207X(98)00131-6
[17] M. Cengher et al 2016 IEEE Transactions on Plasma Science **44** 3465
https://doi.org/10.1109/TPS.2016.2571219
[18] R.A. Moyer et al 2018 Rev. Sci. Instrum. **89** 10E106
https://doi.org/10.1063/1.5038350
[19] M. A. Van Zeeland et al 2004 Rev. Sci. Instrum. **75** 3423
https://doi.org/10.1063/1.1786641
[20] J. Chen et al 2016 Rev. Sci. Instrum. **87** 11E108
https://doi.org/10.1063/1.4960056
[21] M.E. Austin et al 2003 Rev. Sci. Instrum. **74** 1457
https://doi.org/10.1063/1.1530387